Eur. Phys. J. B **1**, 523–531 (1998)

THE EUROPEAN PHYSICAL JOURNAL B

Diffusion of adsorbates on random alloy surfaces

F. Nieto[1,a] and C. Uebing[1,2,b]

[1] Max-Planck-Institut für Eisenforschung, 40074 Düsseldorf, Germany
[2] Lehrstuhl für Physikalische Chemie II, Universität Dortmund, 44227 Dortmund, Germany

Received: 24 October 1997 / Accepted: 17 December 1997

Abstract. In this work the diffusion of non-interacting adsorbates on a random AB alloy surface is considered. For this purpose a simple cubic (sc), body-centered cubic (bcc) or face-centered cubic (fcc) auxiliary metal lattice is introduced. The auxiliary lattice is truncated parallel to its (100) plane in such a way that the fourfold hollow positions of the metal surface form a regular net of adsorption sites with square symmetry. The adsorption energy of each adsorption site is determined by its own environment, *i.e.* by the numbers of direct A or B neighbors. The Monte-Carlo method has been utilized to simulate surface diffusion of adsorbates on such energetically heterogeneous alloy surfaces and to calculate the tracer, jump and chemical diffusion coefficients. The chemical diffusion coefficient was calculated *via* two different approaches: the fluctuation and the Kubo-Green method. The influence of energetical heterogeneities on the surface diffusion is largely pronounced at low temperatures and low surface coverages, where most of the adatoms are trapped by deep adsorption sites. It was found that at low temperatures the sequential occupation of the different types of adsorption sites can be observed.

PACS. 68.35.Fx Diffusion; interface formation – 68.35.Bs Surface structure and topography – 68.35.-p Solid surfaces and solid-solid interfaces

1 Introduction

Diffusion of adsorbed particles on heterogeneous surfaces is probably one of the most important surface processes and occurs in a great number of technical devices such as gas separation and purification tubes, in automotive catalysis, *etc.* The detailed understanding of such processes is essential for technological improvements but appears to be also very important from the fundamental aspects of basic science.

In recent years the development and improvement of powerful experimental techniques for surface analysis on the atomic scale has substantially improved our knowledge about the energetic surface topography. Systematic studies have encouraged the development of adequate refined atomistic models for heterogeneous surfaces capable of including the energetic surface topography in the statistical description of heterogeneity [1–13]. Surface diffusion on heterogeneous (and on homogeneous surfaces as well) is a many particle process. The exact analytical calculation of diffusion coefficients is possible only for a few exceptional cases (*e.g.* for noninteracting lattice gases). However, in more realistic cases analytical expressions cannot be derived and Monte-Carlo simulations have proven to be an adequate and powerful tool to study surface diffusion in the framework of the lattice-gas scheme [14–16].

In the present paper we characterize surface diffusion of non-interacting adsorbates on the energetically heterogeneous (100) surface of a random cubic AB alloy. It is assumed that the characteristics of the adsorption sites are determined by the relative local concentration of A and B species in their direct vicinity. It is quite obvious that the model considered here is highly idealized and is not meant to reproduce a particular experimentally studied system. However, the intention of this work is (1) to identify and characterize the most prominent features of surface diffusion processes for our simple alloy model and (2) to draw general conclusions on the effects of a finite number of different adsorption sites on surface diffusion and (3) to provide a basis for the evaluation of experimental diffusion studies on heterogeneous surfaces.

The paper is organized as follows: in Section 2 we describe in detail the lattice gas model and the Monte-Carlo simulational technique used to obtain the desired diffusion quantities. Results are presented and discussed in Section 3. Finally, we give our conclusions in Section 4.

[a] *Permanent address:* Departamento de Física and Centro Latinoamericano de Estudios Ilya Prigogine, Universidad Nacional de San Luis, CONICET, Chacabuco 917, 5700 San Luis, Argentina
[b] e-mail: `uebing@mpie-duesseldorf.mpg.de`

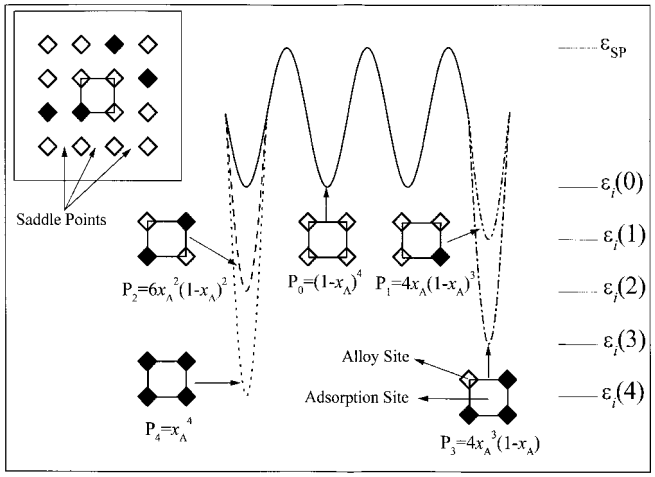

Fig. 1. Schematic representation of the energetic surface heterogeneity for the (100) surface of a random AB alloy. The inset shows the metal lattice built up by A (filled symbols, concentration x_{A}) and B atoms (open symbols, concentration $x_{\mathrm{B}} = 1 - x_{\mathrm{A}}$). The boxes determine single elementary cells of the square lattice. Adatoms may occupy fourfold hollow positions, *i.e.* the centers of the elementary cells. The potential used for the simulation of adatom surface diffusion is also shown. The adsorption energy of each site, $\varepsilon_i(n_{\mathrm{A}})$, depends on its configuration according to equation (2). There are five different adsorption sites with adsorption energies $\varepsilon_i(n_{\mathrm{A}})$ and probabilities $P_{n_{\mathrm{A}}}$.

2 Basic definitions and simulational details

2.1 The lattice-gas model

Let us consider a simple cubic (sc), body-centered cubic (bcc) or face-centered cubic (fcc) metal lattice. The regular sites of this three-dimensional lattice are randomly occupied by only two kinds of metal atoms A and B. Despite its simplicity this model of a random binary AB alloy is well-suited to describe many technologically interesting alloy systems. However, in this work we will consider the AB alloy just as a support for adsorbed species. We assume that the bulk is truncated parallel to the (100) plane in such a way that the topmost layer of the AB alloy forms an unreconstructed surface with square symmetry. This two-dimensional auxiliary lattice of randomly arranged A and B atoms form a square net (or lattice) of fourfold hollow sites which are considered to constitute the lattice of adatom adsorption sites (traps). It is trivially to note that if A and B atoms are undistinguishable (*i.e.* chemically identical) this model describes the adsorption of adatoms on a homogeneous metal surface. The presence and random distribution of chemically different A and B atoms in the direct vicinity of every adsorption sites causes an energetic surface heterogeneity which obviously influences the thermally activated surface mobility of adatoms, *i.e.* the surface diffusion.

In Figure 1 the metal atoms occupying the sites of the two-dimensional auxiliary lattice are schematically represented by filled and open symbols, respectively. It is assumed that the concentration of A atoms (for instance the filled symbols) is given by x_{A}. Thus, if vacancies in the metal lattice are not considered , $x_{\mathrm{B}} = 1 - x_{\mathrm{A}}$ is the concentration of B atoms (represented by the empty symbols). As already mentioned we assume that these two species are randomly distributed. Each elementary cell of this lattice (as an example, one of them is shown by a box in the inset of Fig. 1) defines a single adsorption site.

Adjacent adsorption sites are separated by potential wells. Surface diffusion of adatoms requires crossing of these saddle points. As in previous work we assume that the saddle point energies are uniformly given by a fixed value, $\varepsilon_{\mathrm{SP}}$, throughout the whole lattice. However, the depth of the potential at the adsorption site i, the adsorption energy ε_i, depends on the configuration of the site, *i.e.* on the number of A and B atoms present in the corresponding elementary cell. In order to calculate ε_i we introduce pairwise interaction energies between adatoms and A or B atoms, ε_{A} and ε_{B}, respectively. We assume that these interaction energies behave additive, *i.e.*

$$\varepsilon_i(n_{\mathrm{A}}, n_{\mathrm{B}}) = n_{\mathrm{A}}\varepsilon_{\mathrm{A}} + n_{\mathrm{B}}\varepsilon_{\mathrm{B}}. \tag{1}$$

Here n_{A} and n_{B} describe the number of A and B atoms on metal sites in the direct vicinity of the corresponding adsorption site (nearest neighbor (NN) sites). It is important to note that we consider only those NN metal atoms which are located within the topmost metal layer [17]. For our square surface we therefore have $n_{\mathrm{A}} + n_{\mathrm{B}} = 4$ and, if $\varepsilon_{\mathrm{A}} \neq \varepsilon_{\mathrm{B}}$, there are five energetically different adsorption sites. Without loss of generality we assume $\varepsilon_{\mathrm{B}} = 0$:

$$\varepsilon_i(n_{\mathrm{A}}, n_{\mathrm{B}}) \equiv \varepsilon_{n_{\mathrm{A}}} = n_{\mathrm{A}}\varepsilon_0 \tag{2}$$

where $\varepsilon_0 = \varepsilon_{\mathrm{A}} > 0$ is a constant and $n_{\mathrm{A}} = 0 \ldots 4$. The choice of $\varepsilon_{\mathrm{A}} > \varepsilon_{\mathrm{B}}$ causes the fully A-coordinated adsorption sites to be the energetically most favorable sites for adatoms.

The characteristic features of our adsorption lattice are schematically outlined in Figure 1. As already mentioned there are five different kinds of adsorption sites at the alloy surface, for each of them a representative elementary cell is drawn as an illustrative example. The probability of the different adsorption sites depends on the bulk concentration of A atoms x_{A} according to

$$P_{n_{\mathrm{A}}} = \binom{n_{\mathrm{A}}}{4} x_{\mathrm{A}}^{n_{\mathrm{A}}}(1 - x_{\mathrm{A}})^{4-n_{\mathrm{A}}} = \binom{n_{\mathrm{A}}}{4} x_{\mathrm{A}}^{n_{\mathrm{A}}}(x_{\mathrm{B}})^{n_{\mathrm{B}}}. \tag{3}$$

In the present work we will investigate the effects of the energetical surface heterogeneity on the surface diffusion of adatoms. For this purpose we will study the most simplest case of non-interacting adatoms on the energetically heterogeneous square surface outlined above. Thus the lattice-gas Hamiltonian of the adatoms can be written as:

$$H = -\sum_{i}^{N} c_i\varepsilon_i, \tag{4}$$

where ε_i is given by equation (2) and the occupation of lattice sites by adsorbates is described by local occupation

variables c_i defined as

$$c_i = \begin{cases} 1, & \text{if site } i \text{ is occupied} \\ 0, & \text{if site } i \text{ is vacant.} \end{cases} \quad (5)$$

Double occupancy of lattice sites is excluded.

It is quite obvious that the model outlined above is highly idealized. Especially the restriction to non-interacting adatoms is rather unrealistic in most cases. However, we would like to emphasize that (a) this model is not meant to reproduce a particular experimental system and (b) the intention of the present work is to investigate the effect of energetically surface heterogeneity on diffusion. At this point it is also important to note that the possibility of adatom-induced surface reconstructions are completely ignored in the present work.

2.2 The Monte-Carlo algorithm

In our Monte-Carlo algorithm the model given by equations (2, 4) is simulated by two interpenetrating $L \times L$ square sublattices with periodic boundary conditions. In the first lattice, the metal auxiliary lattice, a fraction x_{A} of lattice sites is preoccupied at random by A atoms while the remaining sites host B atoms. Then, this rigid distribution of metal atoms is used to calculate site specific adsorption energies ε_i in the second, the adatom lattice, according to equation (2). Finally, an initial adatom configuration is generated by throwing θL^2 particles at random on the adatom sublattice. Here θ denotes the desired adatom coverage.

The MC simulation of surface diffusion is performed in the canonical ensemble applying the Metropolis importance sampling algorithm [18,19]. We assume that the elementary steps of surface diffusion are jumps of adsorbed particles from occupied initial sites i to empty nearest neighbor sites j. In essence, the energy barrier which needs to be overcome by diffusing particles, is given by the energy difference between saddle point energy (*i.e.* the maximum potential energy along the trajectory of a jumping adatom) and the initial adsorption energy,

$$\Delta\varepsilon_i = \varepsilon_{\mathrm{SP}} - \varepsilon_i = \varepsilon_{\mathrm{SP}} - n_{\mathrm{A}}\varepsilon_0. \quad (6)$$

The associated jump probabilities, P_i^{J} are given by [8]

$$P_i^{\mathrm{J}}(n_{\mathrm{A}}) = \frac{1}{\kappa} \exp\left[-\frac{\Delta\varepsilon_i}{k_{\mathrm{B}}T}\right] \quad (7)$$

with κ as normalization factor. κ essentially determines the time in which an adsorbed atom is allowed to attempt a jump, as explained in detail in reference [3]. In order to optimize the computational time of a Monte-Carlo algorithm a suitable choice of κ is indispensable. An obvious choice would be

$$\kappa = \kappa_{\max} = \exp\left(-\frac{\Delta\varepsilon_i(\min)}{k_{\mathrm{B}}T}\right). \quad (8)$$

Here $\Delta\varepsilon_i(\min)$ represents the activation energy for the most favorable physically realizable jump [8]. This choice avoids jump events with $P_j > 1$ and has been used throughout this work.

The jump algorithm used in the present work has been discussed in detail in [8] and will be summarized only briefly: first, an initial site i of the adatom lattice is picked at random, if filled, an adjacent final site j is randomly selected. If the destination is vacant, a jump can occur with the probability P_i^{J} given by equation (7), otherwise no jumps occurs. One Monte-Carlo step (MCS) corresponds to L^2 interrogations (in random order) of adatom lattice sites.

Before starting a diffusion run a desired temperature T was established and a large number of initial MCS's were performed to reach thermodynamical equilibrium. As in reference [8] approach to equilibrium is monitored by following the total energy and is assumed to occur when this quantity starts to fluctuate about an average value. The time (in units of MCS's) needed for equilibration depends on lattice size, temperature and coverage. Typically 5×10^3 MCS are required to establish equilibrium in lattices containing up to 64×64 sites. In order to obtain accurate values of the desired surface diffusion coefficients (to be discussed below), diffusion runs of up to 6×10^4 MCS's for up to 136 different initial configurations were performed. These simulations were carried out using the supermassive parallel Intel Paragon supercomputer of the Jülich research center.

2.3 Determination of surface diffusion coefficients

After approaching thermodynamical equilibrium, we have measured the tracer surface diffusion coefficient D^* by following the non-correlated random-walk of $N = \theta L^2$ tagged particles. D^* is defined through the generalized definition

$$D^* = \lim_{t\to\infty}\left[\frac{1}{2dt}\left\langle|\mathbf{R}_i(t) - \mathbf{R}_i(0)|^2\right\rangle\right] \quad (9)$$

where d is the Euclidean dimension, (in the case of surface diffusion $d = 2$); the vector $\mathbf{R}(t)$ determines the position of a tagged particle at time t, and $(\mathbf{R}(t) - \mathbf{R}(0))^2$ is its mean square displacement, which is expressed in units of the lattice constant. The tracer diffusion coefficient is a single particle diffusion coefficient. However, in the course of Monte-Carlo simulations it is quite useful to average over all N particles according to

$$D^* = \lim_{t\to\infty}\left[\frac{1}{2dNt}\sum_{i=1}^{N}\left\langle|\mathbf{R}_i(t) - \mathbf{R}_i(0)|^2\right\rangle\right]. \quad (10)$$

We note that the tracer diffusion coefficient can be defined as the product of a tracer correlation factor f [20, 21], a vacancy availability factor V, and an average jump probability $\langle P^{\mathrm{J}}\rangle$ [22,23],

$$D^* = fV\langle P^{\mathrm{J}}\rangle. \quad (11)$$

The chemical diffusion coefficient D, which is a many particle diffusion coefficient, is determined *via* two different approaches, the fluctuation method and the Kubo-Green method.

In essence, the fluctuation method measures the particle number autocorrelation function, $f_n(t)/f_n(0)$, for a small probe region embedded in the whole two dimensional lattice. The ratio $f_n(t)/f_n(0)$ is then compared with the theoretical curve [24,25], yielding D, which we call D_{F}. Thus, this method is a computer simulation of the field emission fluctuation method [24] used experimentally to determine adsorbate diffusion coefficients.
For the autocorrelation function, we can write

$$\frac{f_n(t)}{f_n(0)} = \frac{\langle \delta N(t) \delta N(0) \rangle}{\langle (\delta N^2) \rangle} \,. \tag{12}$$

Here N is the number of adatoms in the probe area. $\left\langle (\delta N)^2 \right\rangle$ is the mean square number fluctuation in an area A containing $\langle N \rangle$ particles. Details of this method are presented in references [16,26]. In the present work we use a 8×8 and 16×16 square probes for the determination of D_{F}.

The second method for determining the chemical diffusion coefficient is based on the Kubo-Green equation, which we write here as [27]

$$D_{\mathrm{KG}} = \left(\frac{\partial \left[\mu / k_{\mathrm{B}} T \right]}{\partial \ln \theta} \right) D_{\mathrm{J}}. \tag{13}$$

Here μ is the chemical potential. D_{J} is the jump diffusion coefficient given by [1]

$$D_{\mathrm{J}} = \lim_{t \to \infty} \left[\frac{1}{2dNt} \left\langle \left(\sum_{i=1}^{N} |\mathbf{R}_i(t) - \mathbf{R}_i(0)| \right)^2 \right\rangle \right]. \tag{14}$$

The jump diffusion coefficient (sometimes also referred to as kinetic factor) is a many particle diffusion coefficient.

The thermodynamic factor of equation (13) is obtained in either one of its two equivalent forms

$$\left(\frac{\partial \left[\mu / k_{\mathrm{B}} T \right]}{\partial \ln \theta} \right)_T = \left[\frac{\left\langle (\delta N)^2 \right\rangle}{\langle N \rangle} \right]^{-1}, \tag{15}$$

either *via* the differentiation of adsorption isotherms obtained in the grand canonical ensemble or *via* the normalized mean square fluctuations $\left\langle (\delta N)^2 \right\rangle / \langle N \rangle$ obtained in the canonical ensemble.

As in previous studies [8,28], the various diffusion coefficients are normalized with respect to D_0, the chemical diffusion coefficient of Langmuir gas.

3 Results and discussion

In this section we will present and discuss the results of Monte-Carlo simulations in order to demonstrate the influence of the energetical surface heterogeneity on the thermodynamical and kinetical properties of adatoms on the (100) surface of a random AB alloy. We will start with a description of purely thermodynamical aspects (Sect. 3.1). Then, in Section 3.2 the emphasis will be on the surface diffusion of adatoms on energetically heterogeneous alloy surfaces.

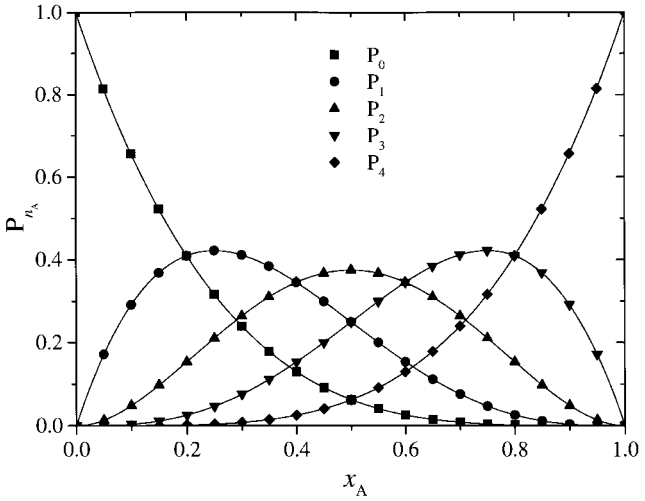

Fig. 2. The probabilities of the different adsorption sites, $P_{n_{\mathrm{A}}}$ *versus* x_{A}. Symbols denote Monte-Carlo results. The solid lines represent the theoretical predictions according to equation (3). The statistical errors are smaller than the size of the symbols used.

3.1 Partial coverages, adsorption isotherms and the thermodynamic factor

As already mentioned the (100) surface of a random AB alloy is assumed to consist of five different adsorption sites. In Figure 2 the probabilities of these sites, $P_{n_{\mathrm{A}}}$, are shown *versus* composition of the AB alloy. The solid lines represent the theoretical predictions according to equation (3). As is intuitively expected for low A bulk concentrations, $x_{\mathrm{A}} \to 0$, fully B-coordinated adsorption sites dominate, and *vice versa*. At intermediate bulk concentrations, $0.2 \lesssim x_{\mathrm{A}} \lesssim 0.8$, mixed-coordinated adsorption sites prevail. In order to test the statistical accuracy of our numerical algorithm we have also calculated $P_{n_{\mathrm{A}}}$ *via* Monte-Carlo simulations (symbols). As expected the agreement between theory and MC data is excellent.

The coverage dependent distribution of adatoms on the different adsorption sites is shown in Figure 3 for different characteristic temperatures and a fixed value of $x_{\mathrm{A}} = 0.2$. In the absence of adatom-adatom interactions the exact solution of this problem can be obtained from classical thermodynamics. Let us define $\theta_{n_{\mathrm{A}}}$ ($n_{\mathrm{A}} = 0 \ldots 4$) as the fraction of occupied sites with energy $\varepsilon_{n_{\mathrm{A}}}$ ($n_{\mathrm{A}} = 0 \ldots 4$). For the calculation of site specific surface coverages, θ_i, as a function of total coverage θ the chemical potentials of adatoms on the various adsorption sites $\mu_{n_{\mathrm{A}}}$ ($n_{\mathrm{A}} = 0 \ldots 4$)

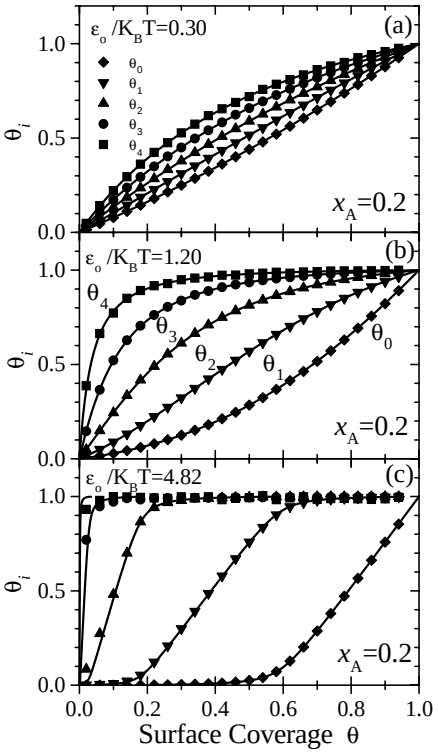

Fig. 3. Site specific adatom coverages, θ_i (symbols), *versus* total adatom coverage θ for three different characteristic temperatures expressed in terms of $\varepsilon_0/k_{\rm B}T$: (a) 0.30, (b) 1.20 and (c) 4.82. Results are shown for a fixed bulk composition, $x_{\rm A} = 0.2$. Symbols denote Monte-Carlo results, while solid lines represent thermodynamical calculations according to equations (16, 17). The statistical errors are smaller than the size of the symbols used.

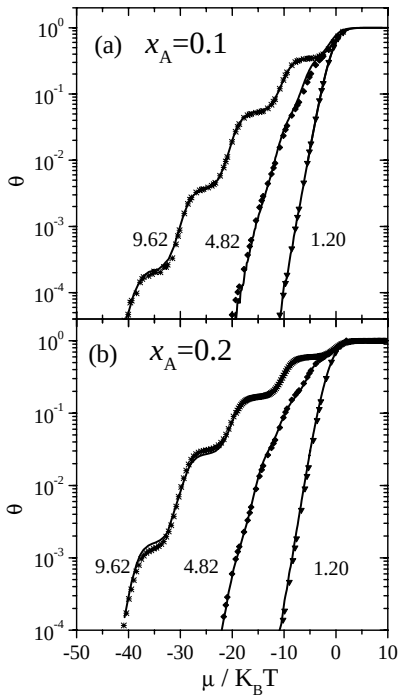

Fig. 4. Adsorption isotherms *i.e.* surface coverage θ *versus* reduced chemical potential $\mu/k_{\rm B}T$ for two different values of $x_{\rm A}$ as indicated. The different curves are labelled according to their temperature (expressed in terms of $\varepsilon_0/k_{\rm B}T$). Monte-Carlo results are represented by symbols. The solid lines are calculated by solving equations (16, 17). The statistical errors are smaller than the size of the symbols used.

is expressed according to

$$\mu_{n_{\rm A}} = \mu_0 - \varepsilon_{n_{\rm A}} + k_{\rm B}T \ln\left(\frac{\theta_{n_{\rm A}}}{1-\theta_{n_{\rm A}}}\right). \qquad (16)$$

Here μ_0 is the chemical potential of the noninteracting Langmuir gas. At thermodynamical equilibrium the chemical potentials are equal ($\mu_{n_{\rm A}} \equiv \mu$) and the total coverage, θ, is given by

$$\theta = \sum_{i=0}^{4} P_{n_{\rm A}} \theta_{n_{\rm A}}, \qquad (17)$$

where the values of $P_{n_{\rm A}}$ are given by equation (3). The system of equations (16, 17) is solved numerically to yield the coverage dependence of the site specific surface coverages, $\theta_{n_{\rm A}}(\theta)$. These quantities are shown in Figure 3. There is an excellent agreement between Monte-Carlo results (symbols) and theoretical values (solid lines) again indicating the statistical accuracy of the MC algorithm.

The data shown in Figure 3 indicate that for a given total coverage θ the site specific coverages $\theta_{n_{\rm A}}$ increase with increasing $n_{\rm A}$. These differences are enhanced upon decreasing the temperature. At low temperatures the sequential occupation of the different sites can be observed, Figure 3c. In fact, at very low coverages only the deepest adsorption sites, θ_4, are occupied while the other sites remain empty. Then after saturation of these sites ($\theta_4 \approx 1$) the occupation of the next type of sites (θ_3) starts while the less deeper sites still remain empty. The sequential occupation of adsorption sites dominates the behavior of the system at low temperatures as is discussed in detail below.

The calculation of adsorption isotherms is also possible by solving equations (16, 17). The results of this procedure are shown in Figure 4 for three different temperatures and for two values of the bulk composition $x_{\rm A}$. At low temperatures, $\varepsilon_0/k_{\rm B}T = 9.82$, the isotherms exhibit a steplike structure consistent with the sequential occupation of different adsorption sites.

According to equation (15) the thermodynamic factor can be obtained *via* the differentiation of adsorption isotherms such as shown in Figure 4. The result of this procedure is presented in Figure 5 and clearly demonstrates that the thermodynamic factor presents sharp peaks which are largely pronounced at low temperatures. These peaks are attributable to the steps (*i.e.* the flat regions) of the corresponding adsorption isotherms (Fig. 4).

Adsorption isotherms and the thermodynamic factor are accessible also *via* MC simulations in the grand canonical ensemble (the method used to calculate them is well

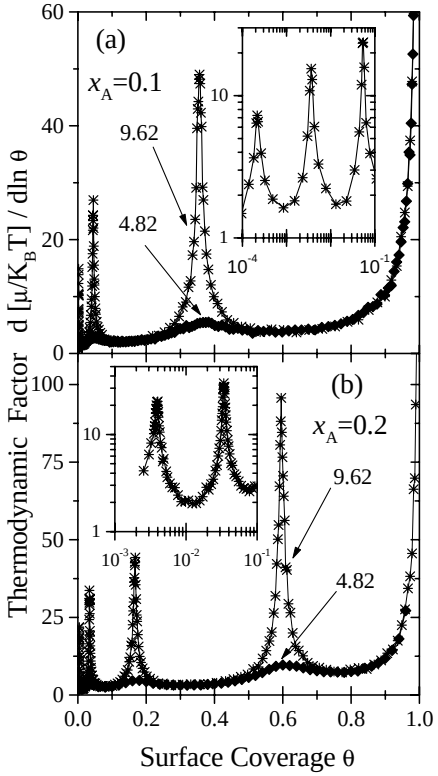

Fig. 5. Thermodynamic factor calculated *via* the numerical differentiation of adsorption isotherms according to equation (15) *versus* surface coverage θ for two different values of x_A as indicated. The temperature is expressed in terms of ε_0/k_BT. The symbols denote the results of MC simulations in the grand canonical ensemble. The statistical errors are smaller than the size of the symbols used.

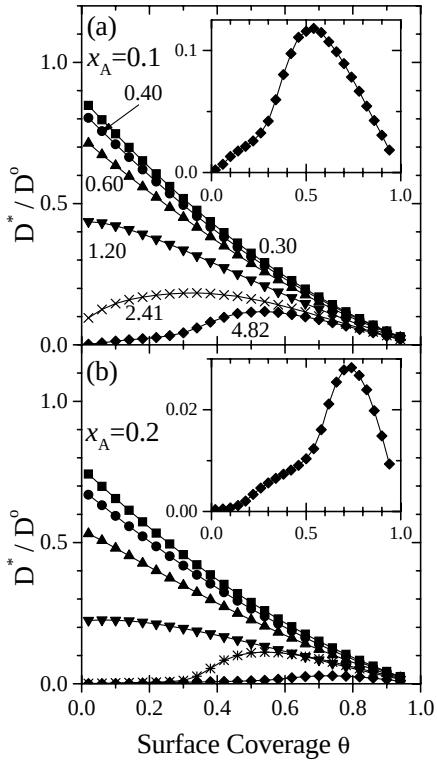

Fig. 6. Normalized tracer diffusion coefficient D^* *versus* total coverage θ for two different values of x_A; (a) $x_A = 0.1$, (b) $x_A = 0.2$. Shown are results for different temperatures expressed in terms of ε_0/k_BT. The insets show the curves for $\varepsilon_0/k_BT = 4.82$. As in previous studies [8,28], the diffusion coefficients are normalized with respect to D_0, the chemical diffusion coefficient of Langmuir gas. The statistical errors are smaller than the size of the symbols used.

discussed in Ref. [29]). Figure 5 clearly demonstrates that the agreement between exact calculations (lines) and simulations (symbols) is excellent.

3.2 Surface diffusion

In this section we will focus on the analysis of the coverage dependence of the tracer and chemical surface diffusion coefficients and related quantities. Figure 6 shows Monte-Carlo results for the normalized tracer diffusion coefficient D^*/D_0 for different values of T and x_A, respectively. From a first inspection of Figure 6 it is intuitively obvious that the effect of the surface heterogeneity is markedly pronounced at low temperatures. At relatively high temperatures, $\varepsilon_0/k_BT = 0.30$, the normalized tracer diffusion coefficient decreases monotonic upon increasing the total surface coverage θ. Even at low values of x_A ($x_A = 0.1$ (Fig. 6a)), the absolute values of D^*/D_0 are slightly reduced with respect to the Langmuir case indicating that tracer diffusion is slowed down as adatoms are adsorbed (and trapped) at the deeper adsorption sites. We note that for the Langmuir case, which is to be expected as $T \to \infty$ (noninteracting limit), the tracer diffusion coefficient is a monotonic function of surface coverage given by (see Eq. (11))

$$\frac{D^*}{D^\circ} = fV = f(1-\theta). \tag{18}$$

Here f is the tracer correlation factor [20,21], which for the two-dimensional Langmuir gas is approximately given by $1 - \theta/2$.

Upon decreasing the temperature, the effects of the surface heterogeneity become more pronounced. The normalized tracer diffusion coefficient is no longer a monotonic function of surface coverage but goes through a well pronounced maximum at intermediate coverages (see the inserts of Fig. 6). In order to explain this maximum we note that at low temperatures and coverages, $\theta \lesssim P_4(x_A)$ (see Eq. (3)), most of the adatoms are trapped at the deepest adsorption sites. Surface diffusion requires adatom jumps out of these sites. However, the average jump probabilities $\langle P^J \rangle$ are low and essentially determine the behavior of D^*. After saturation of the deepest adsorption sites, the sequential occupation of higher adsorption sites causes a gradual increase of $\langle P^J \rangle$, which is reflected by a gradual increase of D^*/D°. At higher coverages, *i.e.* where most of the deeper adsorption sites are saturatured, the tracer

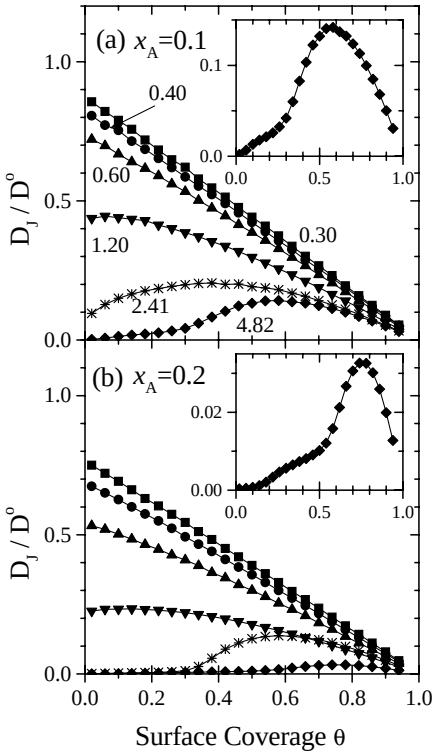

Fig. 7. Same as Figure 6 for the normalized jump diffusion coefficient, D_J/D_0.

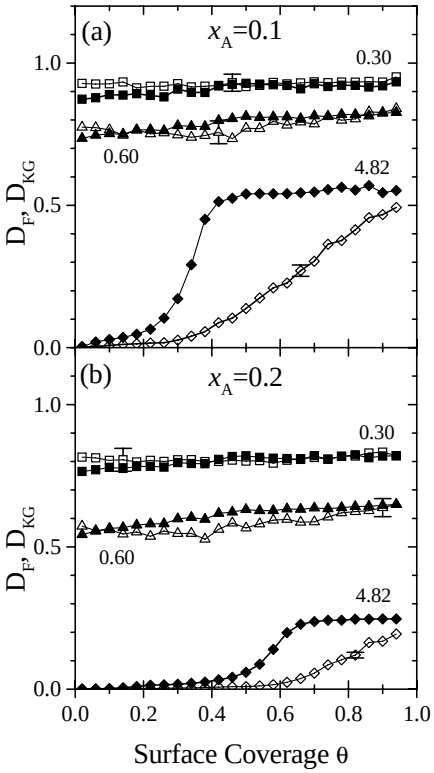

Fig. 8. Chemical diffusion coefficient calculated by the fluctuation method, D_F (open symbols), and by the Kubo-Greem method, D_{KG} (filled symbols), as a function of coverage for two different values of x_A as indicated. Different temperatures expressed in terms of ε_0/k_BT are shown. Error bars are shown to characterize the statistical errors of the Monte-Carlo simulations.

diffusion coefficient goes through a relative maximum and finally decreases to zero as θ approaches unity. This final decrease of D^* at high coverages is intuitively expected as the vacancy availability factor V is very small under such circumstances.

Figure 7 presents the coverage dependence of the normalized jump diffusion coefficient, D_J/D° given by equation (14). It is quite obvious that D^* and D_J behave in a strikingly similar way, despite their substantially different meanings (see Eqs. (9, 14)).

Figure 8 compares the coverage dependence of the chemical diffusion coefficient calculated *via* fluctuation (open symbols) and Kubo-Green method (filled symbols), respectively. At high temperatures both methods show a acceptable agreement. However, significant discrepancies appear at low temperatures.

Discrepancies between D_{KG} and D_F have already been observed for diffusion on homogeneous surfaces in the presence of ad-ad interactions causing first order phase transitions [7] or when the effects of the energetical topography are included [30]. An overall consistent explanation of these findings has been given in reference [30]: the fluctuation method fails when the applicable length scale of the lattice gas system becomes comparable to the probe dimension, or in other words, when the probe misses the long wavelength fluctuations of the particle density. This argument is reinforced by previous results [31] indicating that discrepancies between D_{KG} and D_F in the presence of phase transitions decrease when the size of the probe area used for the calculation of D_F is increased (however, an increase in the probe area produces a costly increase in computing time). Therefore, we conclude that the Kubo-Green method for determining the chemical diffusion coefficient is more appropriate in our case and we will proceed to analyse this quantity.

At high temperatures the chemical diffusion coefficient does not depend much on coverage (Fig. 8). This behavior is similar to that of the homogeneous (*i.e.* Langmuir) case. However, the absolute value of D_{KG} is reduced with respect to the Langmuir gas due to the presence of adatoms adsorbed at sites with different adsorption energies. A very different situation is observed at low temperatures (Figs. 8 and 9c). The D_{KG} *versus* θ curves exhibit two plateaus and low and high coverages, respectively, and a transition regime in between.

In order to explain this behavior we recall that the chemical diffusion coefficient can be expressed as a product of a kinetic (the jump diffusion coefficient) and a thermodynamic factor (Eq. (13)). This process is illustrated in Figure 9. The continuous increase of the jump diffusion coefficient for $\theta \lesssim 0.7$ and its wide peak at $\theta \approx 0.7$ (shown in Fig. 9a) in conjunction with the peaks of the thermodynamic factor (Fig. 9b) together determine the low temperature behavior exhibited by the chemical diffusion coefficient. Figure 9c shows that D_{KG} exhibits

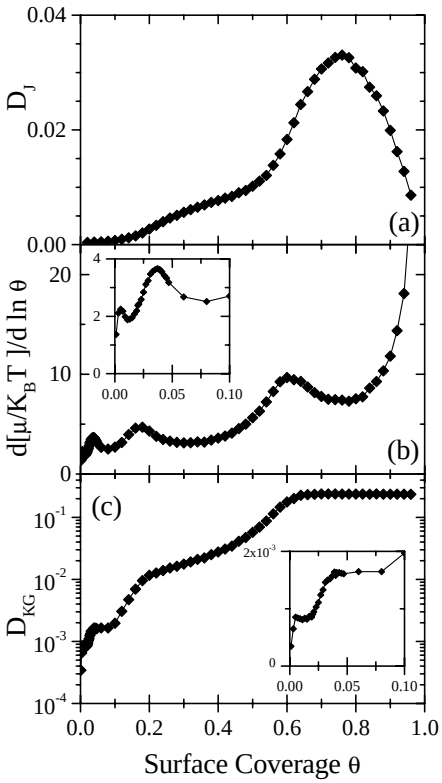

Fig. 9. (a) Jump diffusion coefficient, D_{J}, (b) thermodynamic factor and (c) chemical diffusion coefficient, D_{KG} as a function of coverage for $x_{\mathrm{A}} = 0.2$ and $\varepsilon_0/k_{\mathrm{B}}T = 4.82$. The insets (in (b) and (c)) show the low coverage region. The statistical errors are smaller than the size of the symbols used.

a series of steps which correspond to the peaks of the thermodynamic factor, which in turn represent the sequential occupation of different adsorption sites.

4 Conclusions

In this work we have considered the diffusion of adsorbates on a random AB alloy surface. For this purpose we have introduced a simple cubic (sc), body-centered cubic (bcc) or face-centered cubic (fcc) auxiliary metal lattice, which is truncated parallel to its (100) plane in such a way that the fourfold hollow positions of the metal surface form a regular net of adsorption sites with square symmetry. The adsorption energy of each adsorption site is determined by its own environment, *i.e.* by the numbers of direct A or B neighbors. This model is probably the simplest realization of an energetically heterogeneous alloy surface. Although this model is highly idealized it is possible and useful to study the general trends and peculiarities of adsorbate diffusion on such surfaces.

The work presented here has clearly shown that surface heterogeneities strongly influence adsorbate diffusion. The effects are largely pronounced at low temperatures and low surface coverages, where most of the adatoms are trapped by deep adsorption sites. It was found that at low temperature the sequential occupation of the different types of adsorption sites can be observed. The chemical diffusion coefficient was found to exhibit stepwise increases corresponding to the sequential saturation of different adsorption sites. In contrast, the tracer and jump diffusion coefficients show a continuous increase at low coverages, *i.e.* when the more stable adsorption sites are filled. Upon increasing the coverage both quantities pass through a relative maximum which is explained by the decrease of the vacancy availability factor V.

It is a pleasure to acknowledge many helpful and stimulating discussions with K. Kehr, V. Pereyra, M. Tringides and G. Zgrablich. This work was made possible by the Heisenberg program of the Deutsche Forschungsgemeinschaft (DFG).

References

1. R. Gomer, Rep. Prog. Phys. **53**, 917 (1990).
2. G. Zgrablich, in *Equilibria and dynamics of gas adsorption on heterogeneous solid surfaces*, edited by W.W. Rudzinski and G. Zgrablich (Elsevier, Amsterdam, 1996).
3. M. Tringides, R. Gomer, Surf. Sci. **145**, 121 (1984).
4. M. Tringides, R. Gomer, Surf. Sci. **155**, 254 (1985).
5. A. Sadiq, K. Binder, Surf. Sci. **128**, 350 (1983).
6. V.P. Zhdanov, Surf. Sci. Lett. **149**, L13 (1985).
7. C. Uebing, R. Gomer, Surf. Sci. **331-333**, 930 (1995).
8. C. Uebing, R. Gomer, J. Chem. Phys. **95**, 7626, 7636, 7641, 7648 (1991).
9. V. Mayagoitia, F. Rojas, V. Pereyra, G. Zgrablich, Surf. Sci. **221**, 394 (1989).
10. M. C. J.L. Riccardo, V. Pereyra, G. Zgrablich, Langmuir **8**, 1518 (1992).
11. V. Mayagoitia, F. Rojas, J.L. Riccardo, V. Pereyra, G. Zgrablich, Phys. Rev. B **41**, 7150 (1990).
12. T.W.K. Mussawisade, K. Kehr, J. Phys.: C **9**, 1181 (1997).
13. Y. Limoge and J.L. Boucquet, Phys. Rev. Lett. **65**, 60 (1990).
14. K. Sapag, V. Pereyra, J.L. Riccardo, G. Zgrablich, Surf. Sci. **295**, 433 (1993).
15. C. Uebing, Phys. Rev. B **49**, 13913 (1994).
16. C. Uebing, R. Gomer, Surf. Sci. **306**, 419 (1994).
17. The restriction to nearest neighbor metal sites within the topmost metal layer is strictly justifiable only for simple cubic lattices where the second nearest neighbor metal atoms are far apart. In principle, for bcc and fcc lattices the metal atoms of the second metal layer should be considered. However, the intention of this paper is to describe the effects of energetical surface heterogeneity on surface diffusion by using the most simplest model, and it is very reasonable to assume that the presence of a fifth nearest neighbor metal atom will certainly influence the absolute values of the corresponding surface diffusion coefficients but will not significantly change the qualitative findings of this work.
18. N. Metropolis *et al.*, J. Chem. Phys. **21**, 1087 (1953).
19. K. Binder, D. Stauffer, in *Applications of the Monte-Carlo Method in Statistical Physics*, edited by K. Binder (Springer-Verlag, Berlin, 1984).

20. A.D. LeClaire, in *Physical Chemistry – An Advanced Treatise*, edited by H. Eyring, D. Henderson, and W. Jost, volume 10 (New York, Academic Press, 1970).
21. G.E. Murch, Philos. Mag. **A 43**, 871 (1981).
22. G.E. Murch, R.J. Thorn, J. Phys. Chem. Solids **38**, 789 (1977).
23. K. Kehr, K. Binder, Simulation of Diffusion in Lattice Gases and Related Kinetic Phenomena, in *Applications of the Monte-Carlo Method in Statistical Physics*, edited by K. Binder, volume 36 of *Topics in Current Physics*, (Berlin, Springer-Verlag, 1987), p. 181.
24. R. Gomer, Surf. Sci. **38**, 373 (1973).
25. G. Mazenko, J.R. Banavar, R. Gomer, Surf. Sci. **107**, 459 (1981).
26. C. Uebing, R. Gomer, Surf. Sci. **317**, 165 (1994).
27. D.A. Reed, G. Ehrlich, Surface Science **102**, 588 (1981).
28. E. Viljoen, C. Uebing, Langmuir **13**, 1001 (1997).
29. A.J. Ramirez-Pastor, M.S. Nazzarro, J.L. Riccardo, G. Zgrablich, Surf. Sci. **341**, 249 (1995).
30. C. Uebing, V. Pereyra, G. Zgrablich, Surf. Sci. **366**, 185 (1996).
31. C. Uebing, R. Gomer, J. Chem. Phys. **100**, 7759 (1994).